Lepton Angular Distributions of Fixed-target Drell-Yan Experiments in Perturbative QCD and a Geometric Approach

Wen-Chen Chang,[1] Randall Evan McClellan,[2,3] Jen-Chieh Peng,[3] and Oleg Teryaev[4]

[1]*Institute of Physics, Academia Sinica, Taipei 11529, Taiwan*
[2]*Thomas Jefferson National Accelerator Facility, Newport News, VA 23606, USA*
[3]*Department of Physics, University of Illinois at Urbana-Champaign, Urbana, Illinois 61801, USA*
[4]*Bogoliubov Laboratory of Theoretical Physics, JINR, 141980 Dubna, Russia*

(Dated: October 31, 2018)

The lepton angular distributions of the Drell-Yan process in fixed-target experiments are investigated by NLO and NNLO perturbative QCD. We present the calculated angular parameters λ, μ, ν and the degree of violation of Lam-Tung relation, $1-\lambda-2\nu$, for the NA10, E615 and E866 experiments. Predictions for the ongoing COMPASS and SeaQuest experiments are also presented. The transverse momentum (q_T) distributions of λ and ν show a clear dependence on the dimuon mass (Q) while those of μ have a strong rapidity (x_F) dependence. Furthermore, λ and ν are found to scale with q_T/Q. These salient features could be qualitatively understood by a geometric approach where the lepton angular distribution parameters are expressed in terms of the polar and azimuthal angles of the 'natural axis' in the dilepton rest frame.

I. INTRODUCTION

The Drell-Yan (D-Y) process [1] is one of the important experimental approaches to explore the partonic structure of hadrons [2]. It is a unique tool of accessing the structures of unstable hadrons such as pions and kaons [3–5]. The D-Y process plays an essential role in probing the sea quarks of protons [6–8] as well. The transverse momentum (q_T) distributions of the D-Y cross sections yield important information on the intrinsic transverse momentum (k_T) distribution of partons [9] in the small-q_T region. Furthermore, the polar and azimuthal angular distributions of leptons produced in unpolarized D-Y process are sensitive to the underlying reaction mechanisms and to the novel parton distributions such as Boer-Mulders functions [10]. For measurement with a transversely polarized target, a recent experiment extracted information on Sivers functions for the first time via the D-Y process [11].

In the rest frame of the virtual photon in the D-Y process, a commonly used expression for the lepton angular distributions is given as [12]

$$\frac{d\sigma}{d\Omega} \propto 1+\lambda\cos^2\theta+\mu\sin 2\theta\cos\phi+\frac{\nu}{2}\sin^2\theta\cos 2\phi, \quad (1)$$

where θ and ϕ refer to the polar and azimuthal angles of l^- (e^- or μ^-). At the leading-order (LO), $q\bar{q}\rightarrow\gamma^*$ with collinear partons leads to a transversely-polarized virtual photon with a prediction of $\lambda=1$ and $\mu=\nu=0$. To describe the D-Y process with finite q_T, higher-order QCD processes, such as $q\bar{q}\rightarrow\gamma^*G$ and $qG\rightarrow\gamma^*q$ in $\mathcal{O}(\alpha_S)$, should be included and these processes could alter the angular coefficients λ, μ and nu. While λ can now deviate from 1, and μ and ν can be nonzero, a well-known result is that the Lam-Tung (L-T) relation [13],

$$1-\lambda-2\nu=0, \quad (2)$$

holds for both NLO processes. Deviation from the L-T relation appears in the NNLO process $\mathcal{O}(\alpha_S^2)$ and beyond, e.g. $q\bar{q}\rightarrow\gamma^*GG$, $qG\rightarrow\gamma^*qG$ and $GG\rightarrow\gamma^*G$ according to pQCD [14].

Violation of the L-T relation was observed in the fixed-target experiments with pion beams by NA10 [3] and E615 [4], while L-T was found to be satisfied in the D-Y production with proton beams by E866 [15]. The q_T range of these fixed-target experiments is between 0 and 5 GeV. As for the measurements of Z boson production in the collider experiments, CDF data of $p-\bar{p}$ collision [16] are consistent with the L-T relation, while CMS and ATLAS data of $p-p$ collision [17, 18] show a clear violation. The violation of L-T relation at $q_T>5$ GeV could be well described taking into account of NNLO pQCD effect [19]. Recently Lambersten and Vogelsang [20] compared the NLO and NNLO pQCD calculations of λ and ν with the data of fixed-target experiments NA10, E615 and E866. Overall the agreement is not as good as seen in the collider data at large q_T.

Recently we interpreted the violation of L-T relation as a consequence of the acoplanarity of the partonic subprocess [21, 22]. This acoplanarity can arise from intrinsic transverse momenta of partons inside the hadrons, or from the perturbative gluon radiation beyond $\mathcal{O}(\alpha_s)$ such that the axis of the annihilating quark-antiquark pair (natural axis) does not reside on the colliding-hadron plane. In addition to the violation of the L-T relation, other salient features of the q_T dependence of the λ, μ and ν parameters of the Z production data from the collider experiments, as well as the rotational invariance properties of these parameters [23], could be well explained by this intuitive geometric approach [21, 22].

In this work we compare the λ, μ, ν data measured at NA10 [3], E615 [4] and E866 [15] with the fixed-order pQCD calculations. The approach is similar to what was done in Ref. [20], but we extend the study to include the L-T violation quantity $1-\lambda-2\nu$, the μ parameter, as well as the scaling behavior of these angular parameters. Furthermore we present the NLO pQCD predictions for the ongoing COMPASS [24] and SeaQuest [25] experiments on the dimuon mass Q and Feynman-x (x_F) dependence of the angular parameters. The common features between the pQCD and the geometric ap-

proach [21, 22] are also discussed.

This paper is organized as follows. In Sec. II, we describe how the fixed-order pQCD calculation is performed to extract the angular distribution parameters. The results from the pQCD calculations for the existing and forthcoming fixed-target experiments are then presented in Sections III and IV, respectively. We further interpret some notable features of pQCD results using the geometric model in Sec. V, followed by conclusion in Sec. VI.

II. CALCULATIONS OF ANGULAR PARAMETERS IN DYNNLO

The formalism of the NLO ($\mathcal{O}(\alpha_S)$) [26] and the NNLO ($\mathcal{O}(\alpha_S^2)$) [27] QCD of the D-Y process have been known for a while. It is not until recently that the packages of evaluating the differential D-Y cross sections up to $O(\alpha_s^2)$ from $p-p$ and $p-\bar{p}$ collisions are available for public usage: DYNNLO [28] and FEWZ [29]. Both packages are the parton-level Monte Carlo programs and they provide the differential cross sections for the D-Y process and W/Z vector boson production. As discussed in Ref. [20], threshold resummation of soft-gluon emission at small q_T is not included in these two packages. Even though resummation is important for the cross sections, it is expected not to affect the angular parameters [30, 31].

In this work we utilize the DYNNLO (version 1.5) package [32]. With some minor modifications, the code can evaluate the D-Y cross sections induced by pion or proton beams on proton or neutron targets. Via the LHAPDF6 framework [33], the parton distribution functions (PDFs) [34] used for the protons and neutrons are "CT14nlo" and "CT14nnlo" in the NLO and NNLO calculations, respectively, and "GRVPI1" for the pion PDFs in both NLO and NNLO calculations. The factorization scale (μ_F) and renormalization scale (μ_R) are set as $\mu_F = \mu_R = Q$.

In order to calculate the λ, μ, and ν parameters, we first calculate the A_i parameters in an alternative expression of the lepton angular distributions of the D-Y process as follows [35]:

$$\frac{d\sigma}{d\Omega} \propto (1+\cos^2\theta) + \frac{A_0}{2}(1-3\cos^2\theta) + A_1 \sin 2\theta \cos\phi + \frac{A_2}{2}\sin^2\theta\cos 2\phi \quad (3)$$

where θ and ϕ, same as in Eq. (1), are the polar and azimuthal angles of l^- (e^- or μ^-) in the rest frame of γ^*. The angular coefficients A_i could be evaluated by the moments of harmonic polynomial expressed as [18, 19]

$$\begin{aligned} A_0 &= 4 - 10\langle\cos^2\theta\rangle, \\ A_1 &= 5\langle\sin 2\theta\cos\phi\rangle, \\ A_2 &= 10\langle\sin^2\theta\cos 2\phi\rangle, \end{aligned} \quad (4)$$

where $\langle f(\theta,\phi)\rangle$ denotes the moment of $f(\theta,\phi)$, i.e. the weighted average of $f(\theta,\phi)$ by the cross sections in Eq. (3).

Experiment	Q (GeV)	x_1	x_F
NA10	$4.05 \le Q \le 8.55$	$0 \le x_1 \le 0.7$	$0 \le x_F$
E615	$4.05 \le Q \le 8.55$	$0.2 \le x_1 \le 1$	$0 \le x_F$
E866	$4.5 \le Q \le 15^*$	$0 \le x_1 \le 0.7$	$0 \le x_F$

* Excluding the Υ region $9 \le Q \le 10.7$ GeV.

TABLE I. Kinematic cuts applied for the experimental acceptance in the fixed-order pQCD calculation.

It is straightforward to show that λ, μ, ν in Eq. (1) are related to A_0, A_1, A_2 via

$$\lambda = \frac{2-3A_0}{2+A_0}; \quad \mu = \frac{2A_1}{2+A_0}; \quad \nu = \frac{2A_2}{2+A_0}. \quad (5)$$

Eq. (5) shows that the L-T relation, $1-\lambda-2\nu = 0$, is equivalent to $A_0 = A_2$.

III. COMPARISON WITH EXISTING DATA FROM NA10, E615 AND E866

Now we compare the results of λ, μ, ν, and the L-T violation, $1-\lambda-2\nu$, from the fixed-order pQCD calculations with existing data from fixed-target experiments. The angular parameters are evaluated as a function of dimuon's q_T in the Collins-Soper frame [35]. We first consider the data from NA10 [3] and E615 [4] for π^- beam interacting with tungsten targets. The NA10 experiment used three different beam energies: 140, 194 and 286 GeV, while E615 utilized a single beam energy of 252 GeV. Since the experiments were done with tungsten targets, the cross sections per nucleon were calculated by the weighted average of the $\pi^- p$ and $\pi^- n$ cross sections with 74 protons and 110 neutrons. Following the experimental acceptance specified in Ref. [20], we apply the kinematic cuts listed in Table I. The results of NLO (red points) and NNLO (blue points) calculations together with the measurements (black points) are shown in Figs. 1, 2, 3, and 4.

Overall, the calculated λ, μ and ν exhibit distinct q_T dependencies. At $q_T \to 0$, λ, μ and ν approach the values predicted by the collinear parton model: $\lambda = 1$ and $\mu = \nu = 0$. As q_T increases, Figs. 1-4 show that λ decreases toward its large-q_T limit of $-1/3$ while ν increases toward $2/3$, for both $q\bar{q}$ and qG processes shown in Ref. [21]. The q_T dependence of μ is relatively mild compared to λ and ν. This is understood as a result of some cancellation effect, to be discussed in Sec. V. Comparing the results of the NLO with the NNLO calculation, $\lambda(\mathrm{NNLO})$ is smaller than $\lambda(\mathrm{NLO})$ while μ and ν are very similar for NLO and NNLO. The L-T violation, $1-\lambda-2\nu$, is zero in the NLO calculation and is nonzero and positive in the NNLO calculation.

As shown in Figs. 1-4, while some general features of the NA10 and E615 data are described by the pQCD calculations, there are notable differences between the data and calculations. From the comparison between them, we find:

1) Perturbative QCD predicts that λ drops as q_T increases, but the data do not show this trend. The expected upper bound

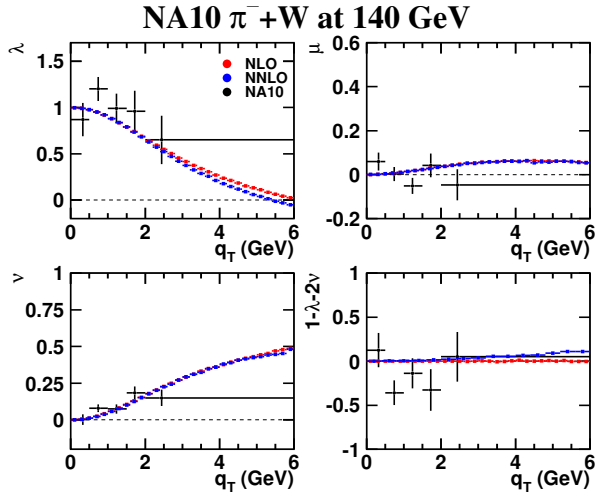

FIG. 1. Comparison of NLO (red points) and NNLO (blue points) fixed-order pQCD calculations with the NA10 $\pi^- + W$ D-Y data at 140 GeV [3] (black points) for λ, μ, ν and $1 - \lambda - 2\nu$.

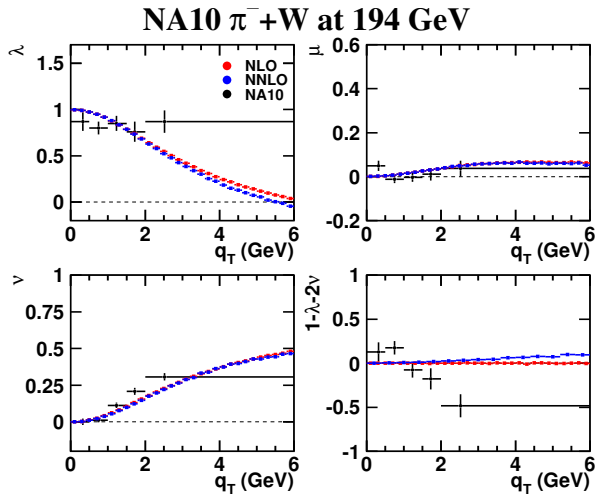

FIG. 2. Same as Fig. 1, but for NA10 data [3] with 194-GeV π^- beam.

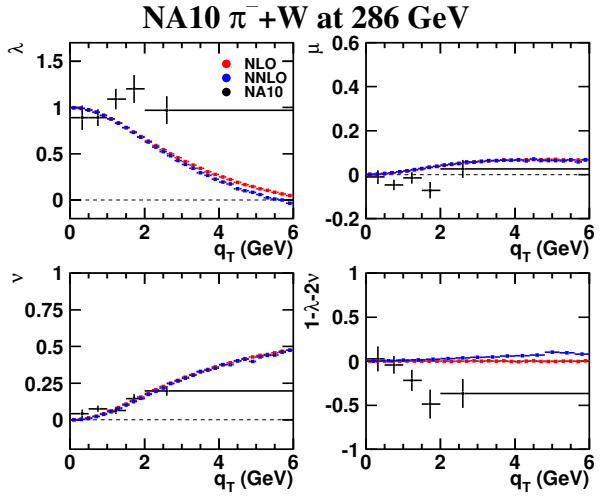

FIG. 3. Same as Fig. 1, but for NA10 data [3] with 286-GeV π^- beam.

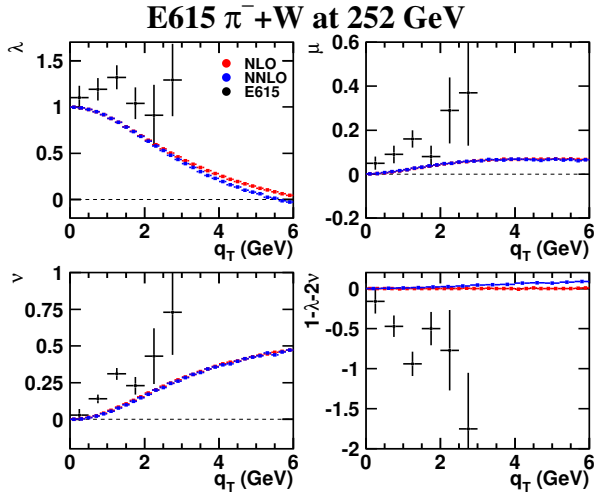

FIG. 4. Comparison of NLO (red points) and NNLO (blue points) fixed-order pQCD calculations with the E615 $\pi^- + W$ D-Y data at 252 GeV [4] (black points) for λ, μ, ν and $1 - \lambda - 2\nu$.

of λ, $|\lambda| \leq 1$, is sometimes exceeded by the data [20]. This could reflect the presence of some systematic uncertainties in the data.

2) The agreement between the data and the pQCD calculation for the μ parameter is quite reasonable for NA10, but less so for E615.

3) The increase of ν with q_T observed in the NA10 data is in good agreement with the pQCD calculation. However, the E615 data are significantly higher than the calculation.

4) The amount of the L-T violation, $1 - \lambda - 2\nu$, for the data is much larger than the prediction from the NNLO pQCD. Moreover, the sign of this violation is negative for the data, but positive for the pQCD. This apparent discrepancy could be partly caused by the un-physical values of λ from the data, as λ should be less than 1.

Regarding these findings two remarks are in order. First, pQCD predicts a sizable magnitude for ν, comparable to the data. Therefore, in order to extract the value of the non-perturbative Boer-Mulders function from the measured data of ν [10, 36, 37], contributions from the pQCD effect must be taken into account. Second, the pQCD calculation for μ tends to overestimate the NA10 data but underestimate the E615 data. As we will see in Sec. IV, μ has a strong dependence on x_F. The incomplete information on the x_F acceptance of the experiments needed for the calculation could contribute to the discrepancy.

The q_T dependencies of the angular distribution parameters of 800-GeV $p+p$ and $p+d$ D-Y are calculated and compared with the E866 measurements [15] in Figs. 5 and 6. Given the large experimental uncertainty, the $p+p$ data in Fig. 5 are not

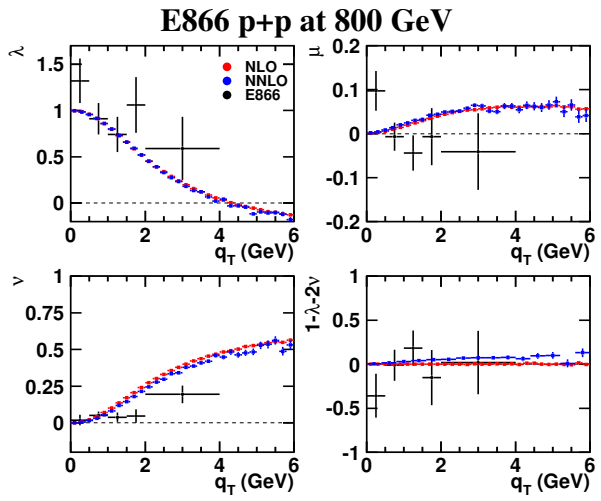

FIG. 5. Comparison of NLO (red points) and NNLO (blue points) fixed-order pQCD calculations with the E866 $p+p$ D-Y data at 800 GeV [15] (black points) for λ, μ, ν and $1-\lambda-2\nu$.

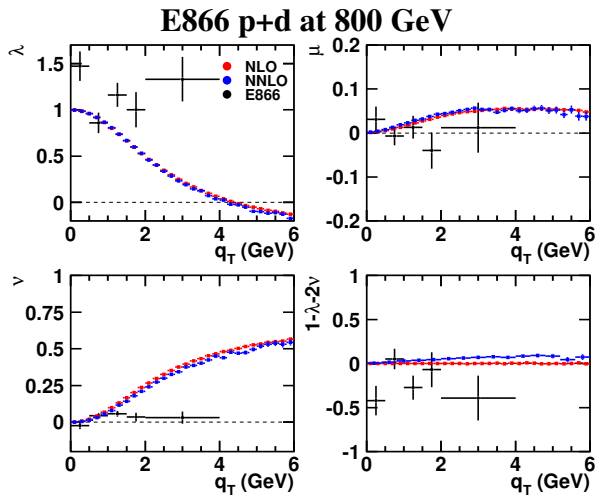

FIG. 6. Same as Fig. 5, but for E866 data [15] with a liquid deuterium target.

in disagreement with the calculation. For Fig. 6, where the $p+d$ data have smaller uncertainties, the agreement between data and the calculation is rather poor. In particular, the data on λ are in general larger than 1, violating the expected upper bound for λ [20].

That the ν data are less than the pQCD prediction in Figs. 5 and 6, suggests a negative contribution from the Boer-Mulders effect in the proton-induced DY. This is opposite to the situation in Fig. 4, where the ν data are more positive than the pQCD, suggesting a positive contribution from the Boer-Mulders function in the pion-induced DY. Since the contribution of the Boer-Mulders effect in ν is proportional to the product of the individual Boer-Mulders functions of quarks and anti-quarks in the colliding hadrons, the proton D-Y data would imply that the sea-quark Boer-Mulders function has a sign opposite to that of the valence Boer-Mulders function in the proton [38]. The pion data from Fig. 4 suggests that the pion valence Boer-Mulders function has the same sign as the proton valence Boer-Mulders function [38].

The NNLO calculations predict a positive $1-\lambda-2\nu$ at NNLO while the data are consistent with zero for the proton target and slightly negative for the deuteron one. The negative values of $1-\lambda-2\nu$ for $p+d$ data are similar to the case for the pion D-Y data shown in Figs. 1-4. In Sec. V, we will discuss why $1-\lambda-2\nu$ must be positive from the perspective of a geometric approach.

IV. PQCD CALCULATIONS FOR THE COMPASS AND SEAQUEST EXPERIMENTS

There are two ongoing fixed-target D-Y experiments which have collected new data on the lepton angular distributions. The first one is the COMPASS experiment at CERN [24], running with 190-GeV π^- beam and transversely-polarized NH_3 target and unpolarized aluminum (Al) and tungsten (W) nuclear targets. The transverse-momentum-dependent Sivers asymmetry in the polarized D-Y process was reported recently [11], and high-statistics unpolarized D-Y data on the W target have also been collected. The second one is the SeaQuest experiment at Fermilab [25], aiming at the measurement of $\bar{d}(x)/\bar{u}(x)$ ratio at intermediate-x region via the D-Y process. It has taken data with 120-GeV proton beam on unpolarized hydrogen, deuterium and various nuclear targets. Both COMPASS and SeaQuest experiments have collected data on the lepton angular distributions of the D-Y process. The final results are expected to be available soon. In addition, the extension of the SeaQuest experiment, the E1039 experiment [39], expects to take more data relevant to the angular distributions in the near future.

Here we present the results of the angular coefficients λ, μ and ν as a function of q_T in various bins of Q and x_F. There are three bins for Q in the range of 4.0–7.0 GeV, as well as three bins for x_F in the range of 0–0.6. These results could be convoluted by the COMPASS and SeaQuest spectrometer acceptances later for a direct comparison with experimental data. Since there are no significant difference between the NLO and NNLO results, we present only the results from the NLO calculation to illustrate the major features.

The mean values of Q and x_F in each bin are listed in Tables II and III. The pQCD calculations show that the $q\bar{q}$ process dominates over the whole q_T region for the π^--induced COMPASS experiment while the qG process becomes more important for $q_T > 1$ GeV in the proton-induced SeaQuest experiment. Through this study, the Q- and x_F-dependencies of λ, μ and ν are also investigated.

Figures 7 and 8 show λ, μ and ν as a function of q_T for various bins of Q and x_F. The q_T distributions of λ and ν parameters depend sensitively on Q, but only weakly on x_F. As for μ, its q_T distribution has strong dependencies on x_F and on Q. In particular, the magnitude of μ is small when x_F is close to 0 and its sign could even turn negative at some q_T region. As x_F increases, the magnitude of μ increases

TABLE II. Mean values of Q and x_F in each Q bin calculated for COMPASS and SeaQuest.

Bin	COMPASS		SeaQuest	
	$\langle Q\rangle$ (GeV)	$\langle x_F\rangle$	$\langle Q\rangle$ (GeV)	$\langle x_F\rangle$
$Q = 4-5$ GeV	4.42	0.32	4.36	0.24
$Q = 5-6$ GeV	5.43	0.32	5.36	0.23
$Q = 6-7$ GeV	6.43	0.32	6.36	0.22

TABLE III. Mean values of Q and x_F in each x_F bin calculated for COMPASS and SeaQuest.

Bin	COMPASS		SeaQuest	
	$\langle Q\rangle$ (GeV)	$\langle x_F\rangle$	$\langle Q\rangle$ (GeV)	$\langle x_F\rangle$
$x_F = 0.0-0.2$	5.01	0.10	4.56	0.10
$x_F = 0.2-0.4$	5.06	0.30	4.55	0.29
$x_F = 0.4-0.6$	5.10	0.49	4.54	0.48

pronouncedly.

In perturbative QCD at $\mathcal{O}(\alpha_S)$, ignoring the intrinsic transverse momenta of the colliding partons, the λ and ν coefficients in the Collins-Soper frame for the $q\bar{q} \to \gamma^* G$ annihilation process [30, 31, 40] and the $qG \to \gamma^* q$ Compton process [3, 41, 42] are given as

$$\lambda = \frac{2Q^2 - q_T^2}{2Q^2 + 3q_T^2} \qquad \nu = \frac{2q_T^2}{2Q^2 + 3q_T^2} \qquad (q\bar{q})$$
$$\lambda = \frac{2Q^2 - 5q_T^2}{2Q^2 + 15q_T^2} \qquad \nu = \frac{10q_T^2}{2Q^2 + 15q_T^2} \qquad (qG), \qquad (6)$$

where q_T and Q are the transverse momentum and mass, respectively, of the dilepton. While the expression for $q\bar{q} \to \gamma^* G$ is exact, that for $qG \to \gamma^* q$ is obtained with some approximation. Equation (6) shows that λ and ν scale with the dimensionless q_T/Q in these pQCD NLO expressions. Nevertheless there is no q_T/Q scaling for the μ parameter in NLO pQCD.

Figures 9 and 10 show the NLO calculations of λ and ν for COMPASS and SeaQuest as a function of the variable q_T/Q in the various Q and x_F bins. The corresponding expressions for the $q\bar{q}$ and qG processes in Eq. (6) are denoted by the solid and dashed lines. Comparing Figs. 9 and 10 with 7 and 8, the λ and ν values for different Q bins now converge into a common curve when they are plotted as a function of q_T/Q. This is consistent with the q_T/Q scaling behavior of Eq. (6).

Figures 9 and 10 also display the fractions of the NLO cross sections due to the $q\bar{q}$ process for COMPASS and SeaQuest. The dominance of the $q\bar{q}$ process in in the π^--induced D-Y in COMPASS explains why the pQCD results for λ and ν are very close to the solid $q\bar{q}$ lines. In contrast, the proton-induced D-Y in SeaQuest has large contributions from the qG process, resulting in the λ and ν closer to the dashed qG lines.

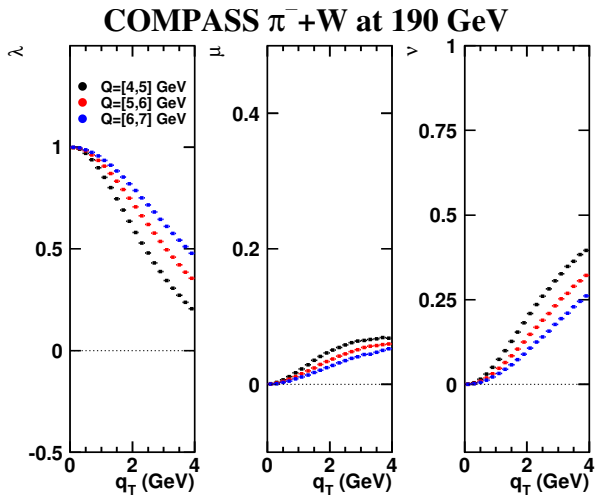

(a)

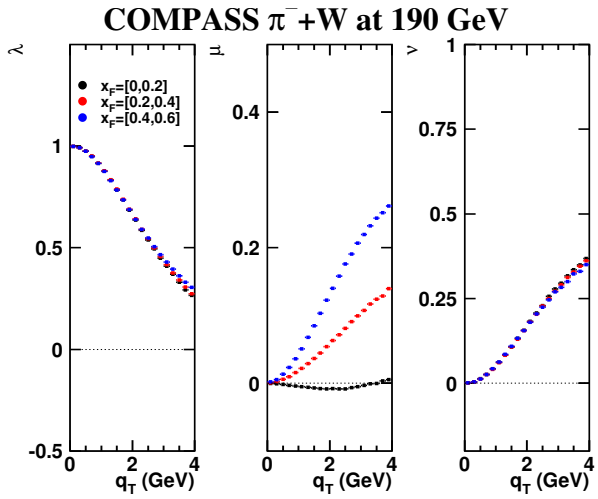

(b)

FIG. 7. (a) NLO pQCD results of λ, μ, and ν as a function of q_T at several Q bins and $x_F > 0$ for D-Y production off the tungsten target with 190-GeV π^- beam in the COMPASS experiment. (b) Same as (a) but at several x_F bins and $4 < Q < 9$ GeV.

In Fig. 11, we plot the q_T distributions of λ, μ and ν in the negative x_F (-0.6 – 0) for COMPASS and SeaQuest. The λ and ν remain the same as that in $x_F > 0$ while μ turns mostly negative.

V. GEOMETRIC MODEL

As seen above, the existing D-Y data of lepton angular distributions can be reasonably well described by the NLO and NNLO pQCD calculations. Various salient features of Q and x_F dependencies as well as q_T/Q scaling are observed in the predicted results of λ, μ and ν parameters for COMPASS and SeaQuest experiments based on NLO pQCD. It is of interest to check if these features could be understood using the geo-

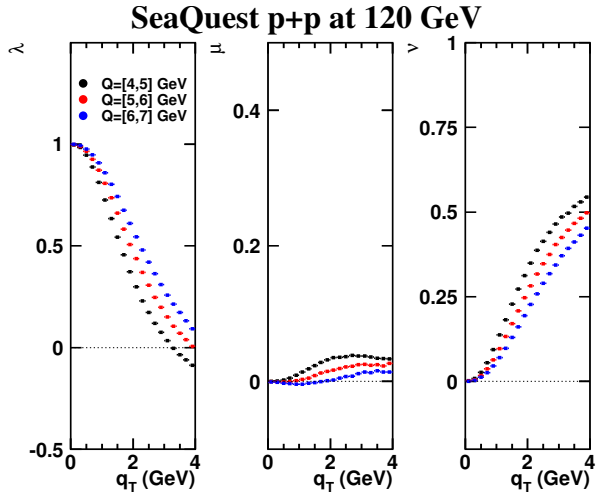

(a)

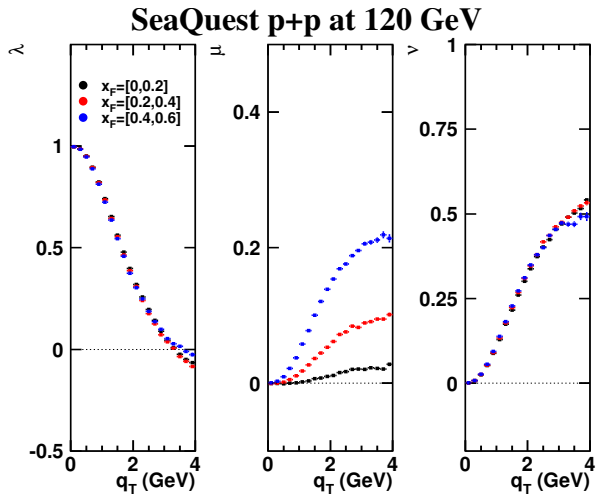

(b)

FIG. 8. (a) NLO pQCD results of λ, μ, and ν as a function of q_T at several Q bins and $x_F > 0$ for D-Y production off the proton target with 120-GeV proton beam in the SeaQuest experiment. (b) Same as (a) but at several x_F bins and $4 < Q < 9$ GeV.

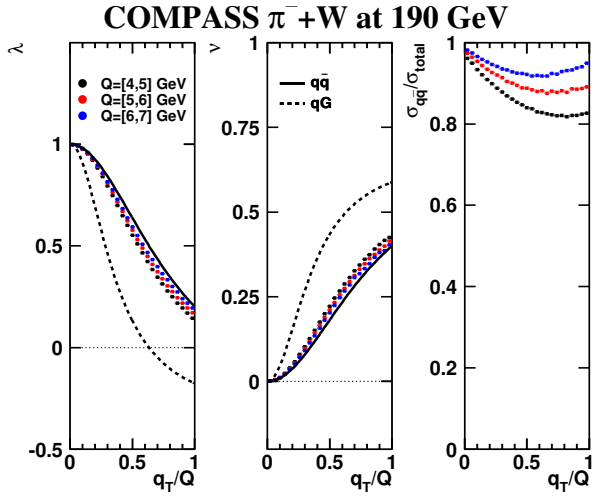

(a)

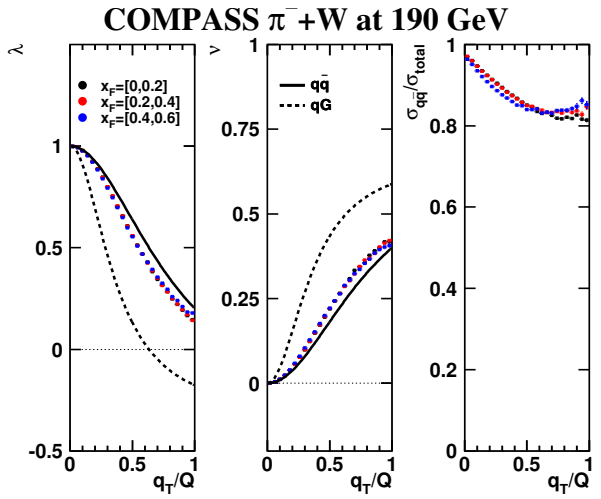

(b)

FIG. 9. (a) NLO pQCD results of λ, ν and the fractions of $q\bar{q}$-process contribution in the total cross sections as a function of scaled transverse momentum q_T/Q for D-Y production off the nuclear tungsten target with 190-GeV π^- beam in the COMPASS experiment. The NLO pQCD expressions of $q\bar{q}$ and qG processes are denoted by the solid and dashed lines respectively. (b) Same as (a) but at several x_F bins and $4 < Q < 9$ GeV.

metric approach developed in Refs. [21, 22].

Here we briefly describe the geometric approach of Refs. [21, 22]. As illustrated in Fig. 12, we define three different planes, the hadron plane, the quark plane, and the lepton plane, in the Collins-Soper frame. In the γ^* rest frame, the beam and target hadron momenta, $\vec{P}_B$ and $\vec{P}_T$ form the "hadron plane" on which the $\hat{z}$ axis, bisecting the $\vec{P}_B$ and $-\vec{P}_T$ vectors, lies. A pair of collinear q and $\bar{q}$ with equal momenta annihilate into a γ^*. The momentum unit vector of q is defined as $\hat{z}'$, and the "quark plane" is formed by the $\hat{z}'$ and $\hat{z}$ axes. Finally, the "lepton plane" is formed by the momentum vector of l^- and the $\hat{z}$ axis. The polar and azimuthal angles of the $\hat{z}'$ axis in the Collins-Soper frame are denoted as θ_1 and ϕ_1. As shown in Refs. [21, 22], the angular coefficients A_i in Eq. (3) can be expressed in term of θ_1 and ϕ_1 as follows:

$$\begin{aligned} A_0 &= \langle \sin^2\theta_1 \rangle \\ A_1 &= \frac{1}{2}\langle \sin 2\theta_1 \cos\phi_1 \rangle \\ A_2 &= \langle \sin^2\theta_1 \cos 2\phi_1 \rangle. \end{aligned} \tag{7}$$

The $\langle \cdots \rangle$ in Eq. (7) is a reminder that the measured values of A_i at a given kinematic bin are averaged over events having particular values of θ_1 and ϕ_1.

As discussed in Refs. [21, 22], up to NLO ($\mathcal{O}(\alpha_S)$) in pQCD, the quark plane coincides with the hadron plane and $\phi_1 = 0$. Therefore $A_0 = A_2$ or $1 - \lambda - 2\nu = 0$, i.e., the

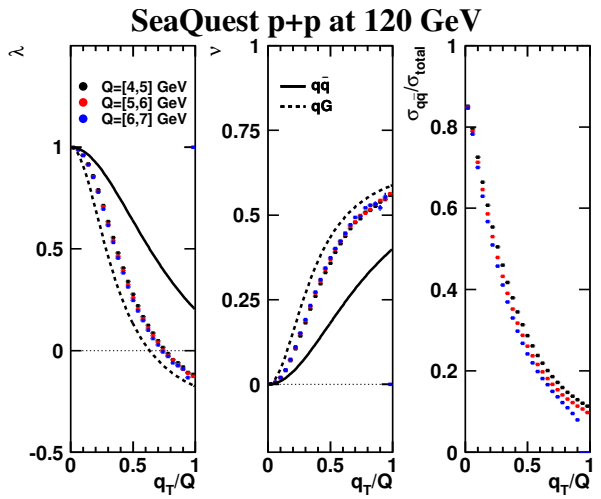

(a)

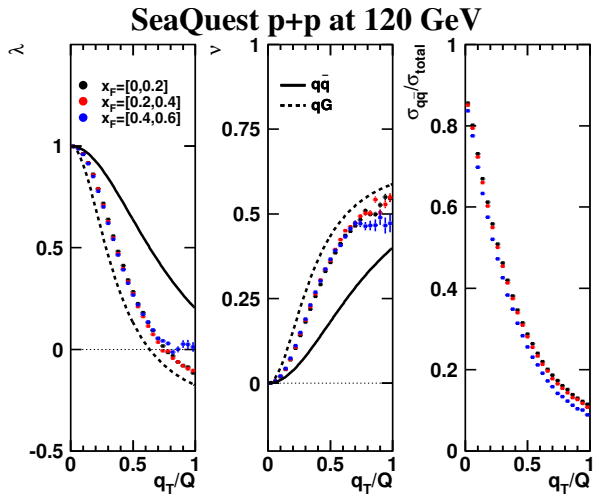

(b)

FIG. 10. (a) NLO pQCD results of λ, ν and the fractions of $q\bar{q}$-process contribution in the total cross sections as a function of scaled transverse momentum q_T/Q for D-Y production off the proton target with 120-GeV proton beam in the SeaQuest experiment. The NLO pQCD expressions of $q\bar{q}$ and qG processes are denoted by the solid and dashed lines respectively. (b) Same as (a) but at several x_F bins and $4 < Q < 9$ GeV. It is noted that the rough structure at large q_T/Q region of the results for x_F =0.4 – 0.6 (blue points) is likely due to the fluctuation of calculations with $Q > 7$ GeV near the edge of the phase space. The structure is expected to be removed, if one requires $Q < 7$ GeV as the top figure.

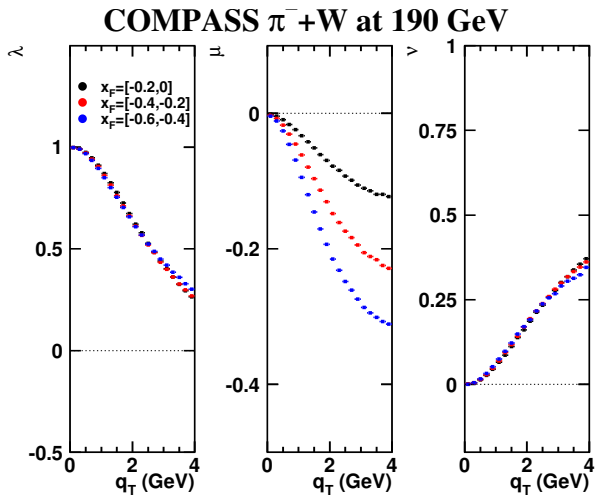

(a)

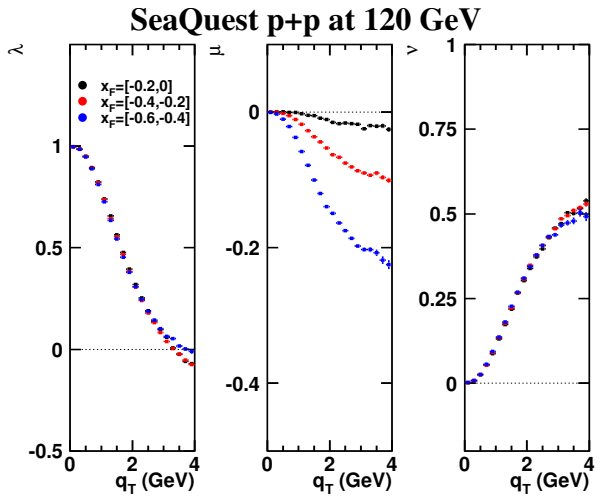

(b)

FIG. 11. (a) NLO pQCD results of λ, μ and ν as a function of transverse momentum q_T at several negative x_F bins and $4 < Q < 9$ GeV for D-Y production off the nuclear tungsten target with 190-GeV proton beam in COMPASS experiment. (b) Same results of (a) for D-Y production off the proton target with 120-GeV proton beam in SeaQuest experiment.

L-T relation is satisfied. Higher order pQCD processes allow the quark plane to deviate from the hadron plane , i.e., $\phi_1 \neq 0$, leading to the violation of L-T relation. For a non-zero ϕ_1, Eq. (7) shows that $A_2 < A_0$. Therefore, when L-T relation is violated, A_0 must be greater than A_2 or, equivalently, $1 - \lambda - 2\nu > 0$. This expectation of $1 - \lambda - 2\nu > 0$ in the geometric approach is in agreement with the results of NNLO pQCD calculations shown in Figs. 1-6. The geometric approach offers a simple interpretation for this result.

Figures 7(b) and 8(b) show that the q_T dependencies for λ and ν are insensitive to the value of x_F. In contrast, the μ parameter depends sensitively on x_F. This striking difference between the λ, μ and ν parameters can be understood in the geometric approach. At the next-to-leading order (NLO), $\mathcal{O}(\alpha_S)$, a hard gluon or a quark (antiquark) is emitted so that γ^* acquires non-zero q_T. Figure 13(a) shows a diagram for the $q - \bar{q}$ annihilation process in which a gluon is emitted from the quark in the beam hadron. In this case, the momentum vector of the quark is modified such that it becomes opposite to the antiquark's momentum vector in the rest frame of γ^* (Fig. 13(b)). Since the antiquark's momentum is the same as the target hadron's momentum, the $\hat{z}'$ axis is along the di-

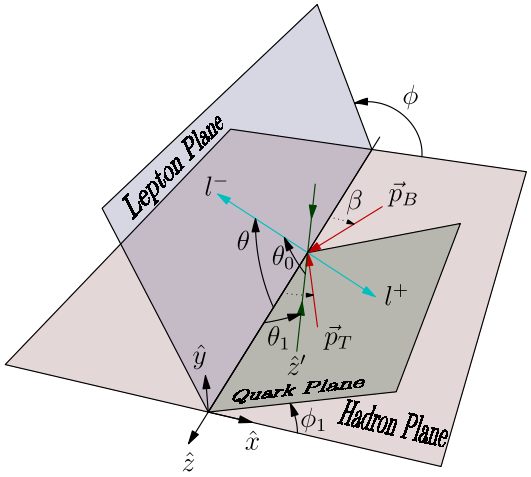

FIG. 12. Definition of the Collins-Soper frame and various angles and planes in the rest frame of γ^*. The hadron plane is formed by $\vec{P}_B$ and $\vec{P}_T$, the momentum vectors of the beam (B) and target (T) hadrons. The $\hat{x}$ and $\hat{z}$ axes of the Collins-Soper frame both lie in the hadron plane with the $\hat{z}$ axis bisecting the $\vec{P}_B$ and $-\vec{P}_T$ vectors. The quark (q) and antiquark ($\bar{q}$) annihilate collinearly with equal momenta to form γ^*, while the quark momentum vector $\hat{z}'$ and the $\hat{z}$ axis form the quark plane. The polar and azimuthal angles of $\hat{z}'$ in the Collins-Soper frame are θ_1 and ϕ_1. The l^- and l^+ are emitted back-to-back with θ and ϕ as the polar and azimuthal angles for l^-.

TABLE IV. Angles θ_1 and ϕ_1 for four cases of gluon emission in the $q-\bar{q}$ annihilation process at order-α_s. The signs of A_0, $A_1(\mu)$, $A_2(\nu)$ for the four cases are also listed.

case	gluon emitted from	θ_1	ϕ_1	A_0	$A_1(\mu)$	$A_2(\nu)$
1	beam quark	β	0	+	+	+
2	target antiquark	β	π	+	−	+
3	beam antiquark	$\pi-\beta$	0	+	−	+
4	target quark	$\pi-\beta$	π	+	+	+

rection of $-\vec{p}_T$. From Fig. 12, it is evident that $\theta_1 = \beta$ and $\phi_1 = 0$ in this case. An analogous diagram in which the gluon is emitted from the antiquark in the target hadron is shown in Fig. 13(c). In this case, $\theta_1 = \beta$ while $\phi_1 = \pi$. Table IV lists the values of θ_1 and ϕ_1 for four cases of different combination of hadron and quark types from which the gluon is emitted [22].

Table IV shows that the sign of μ could be either positive or negative, depending on which parton and hadron the gluon is emitted from. Hence, one expects some cancellation effects for μ among contributions from various processes. Each process is weighted by the corresponding density distributions for the interacting partons. At $x_F \sim 0$, the momentum fraction carried by the beam parton (x_B) is comparable to that of the target parton (x_T). Therefore, the weighting factors for various processes are of similar magnitude and the cancellation effect could be very significant, resulting in a small value of μ. On the other hand, as x_F increases toward 1, x_B becomes much larger than x_T. In this case the weighting factors are now dominated by fewer processes, resulting in less cancellation and a larger value of μ. This explains why the μ parameter exhibits a strong x_F dependence in Figs. 7(b) and 8(b).

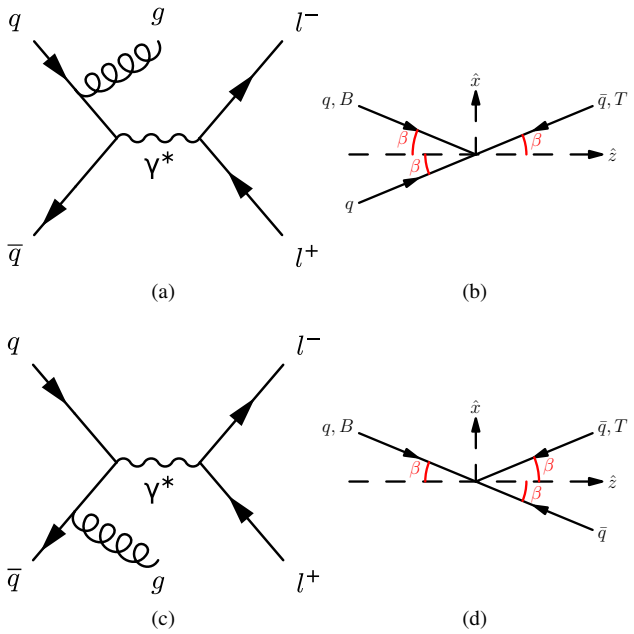

FIG. 13. (a) Feynman diagram for $q-\bar{q}$ annihilation where a gluon is emitted from a quark in the beam hadron. (b) Momentum vectors for q and $\bar{q}$ in the C-S frame before and after gluon emission. The momentum direction of q is now collinear with that of $\bar{q}$. (c) Feynman diagram for the case where a gluon is emitted from an antiquark in the target hadron. (d) Momenta vectors for q and $\bar{q}$ in the C-S frame before and after gluon emission for diagram (c).

Table IV also shows that A_0 and A_2 have the same sign (positive) for all four cases. This implies the absence of x_F-dependent cancellation effect for them. Hence λ and ν have very weak x_F dependencies, as shown in Figs. 7(b) and 8(b). Therefore, the observed strong rapidity dependence for μ and weak rapidity dependence for λ and ν in pQCD calculation can be nicely described by the geometric picture. In addition, considering the strong x_F-dependence for the q_T distribution of μ parameters, it will be instructive for the experiments to measure the q_T dependence of μ at several x_F regions, instead of integrating over the entire x_F.

The NLO pQCD expressions of λ and ν as a function of q_T in Eq. (6) have been derived based on a geometric picture of collision geometry in the parton level [21, 22]. Within the geometric picture, the A_0 and A_2 at NLO are equal to $\langle \sin^2\theta_1 \rangle$ (Eq. (7)) with $\phi_1 = 0$. Given $q_T/Q = \tan\theta_1$ or $-\tan\theta_1$, the scaling of A_0 and A_2 (equivalently λ and ν) with q_T/Q could also be understood.

Figure 14 shows both NLO (red points) and NNLO (blue points) pQCD results of λ, ν and $1-\lambda-2\nu$ as a function of q_T at the kinematic bin of $5 < Q < 6$ GeV and $0.2 < x_F < 0.4$ for the COMPASS experiment. The corresponding NLO pQCD expressions of q_T dependence for $q\bar{q}$ and qG subprocesses in Eq. (6) are drawn as dotted and

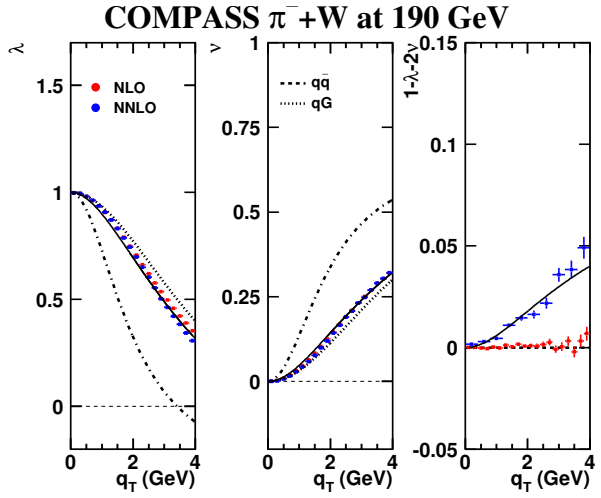

FIG. 14. NLO (red points) and NNLO (blue points) pQCD results of λ, μ, ν and $1-\lambda-2\nu$ as a function of q_T at the kinematic bin of $5 < Q < 6$ GeV and $0.2 < x_F < 0.4$ for D-Y production off the tungsten target with 190-GeV π^- beam in COMPASS experiment.

dotted-dash curves. Assuming the fraction of these two processes is q_T independent, a best-fit to the NNLO results of λ yields the fraction of $q\bar{q}$ process to be 83% for the COMPASS experiment. This value is consistent with pQCD results shown in Fig. 9. Applying this relative fraction of two pQCD processes, the NNLO result of ν could be reasonably well described, as shown in Fig. 14, with the acoplanarity parameter $\langle \cos 2\phi_1 \rangle$, set at 0.94. The predicted q_T distribution of L-T violation $1-\lambda-2\nu$ from the NNLO pQCD could be then nicely described as well.

Overall our studies show that salient features of q_T/Q scaling and x_F dependency for the λ, ν, μ parameters of fixed-target D-Y experiments evaluated by NLO pQCD as well as the L-T violation $1-\lambda-2\nu$ from the NNLO pQCD can be nicely understood using the geometric picture.

VI. SUMMARY AND CONCLUSION

We have presented a comparison of the measurements of the angular parameters λ, μ, ν and $1-\lambda-2\nu$ of the D-Y process from the fixed-target experiments with the corresponding results from the NLO and NNLO pQCD calculations. Qualitatively the transverse momentum q_T dependency of λ, μ and ν in the data could be described by pQCD. The difference between NLO and NNLO results becomes visible at large q_T. The L-T violation part $1-\lambda-2\nu$ remains zero in the NLO pQCD calculation and turns positive in NNLO pQCD. It is contrary to the measured negative values in the pion-induced D-Y experiments NA10 and E615. Additional non-perturbative effects such as Boer-Mulders function may account for the discrepancy.

From the NLO pQCD calculation, we then present the predictions of the angular parameters as a function of q_T in several Q and x_F bins for the ongoing COMPASS and SeaQuest experiments. The λ and ν show some mild dependence on Q and a weak x_F dependence, while μ exhibits a pronounced dependence on x_F. For different x_Fs, λ and ν are predicted to approximately scale with q_T/Q.

The x_F dependency of the angular parameters is well described by the geometric picture. In particular, the weak rapidity dependencies of the λ and ν, and the pronounced rapidity dependency for μ can be explained by the absence or presence of rapidity-dependent cancellation effects. The occurrence of acoplanarity between the quark plane and the hadron plane ($\phi_1 \neq 0$), for the pQCD processes beyond NLO leads to a violation of $L-T$ relation. The predicted positive value of $1-\lambda-2\nu$, or $A_0 > A_2$ when ϕ_1 is non-zero, is consistent with the NNLO pQCD results.

The NLO and NNLO pQCD calculations should provide a good benchmark for understanding the experimental data of lepton angular distributions of fixed-target D-Y experiments. It is interesting to see many salient features present in pQCD results can be readily understood by the geometric picture. This intuitive approach could offer some useful insights on the origins of many interesting characteristics of the lepton angular distributions in the forthcoming new precision data from the COMPASS and SeaQuest experiments. Any deviation from the pQCD results on the L-T violation as well as the ν parameter would indicate the presence of non-perturbative effects such as the Boer-Mulders functions. Finally we emphasize the importance of measuring the angular parameters in D-Y process, which provides a powerful tool to explore the reaction mechanism and parton distributions potentially more sensitive than the D-Y cross sections alone. The measurement of the q_T distributions of μ parameters with x_F dependence is suggested, and the pQCD effect should be included in the extraction of non-perturbative Boer-Mulders effect from the data of ν.

ACKNOWLEDGMENTS

This work was supported in part by the U.S. National Science Foundation and the Ministry of Science and Technology of Taiwan. It was also supported in part by the U.S. Department of Energy, Office of Science, Office of Nuclear Physics under contract DE-AC05-060R23177.

[1] S.D. Drell and T.M. Yan, Phys. Rev. Lett. **25**, 316 (1970); Ann. Phys. (NY) **66**, 578 (1971).
[2] J.C. Peng and J.W. Qiu, Prog. Part. Nucl. Phys. **76**, 43 (2014).
[3] NA10 Collaboration, S. Falciano *et al.*, Z. Phys. C **31**, 513 (1986); M. Guanziroli *et al.*, Z. Phys. C **37**, 545 (1988).

[4] E615 Collaboration, J.S. Conway *et al.*, Phys. Rev. D **39**, 92 (1989); J.G. Heinrich *et al.*, Phys. Rev. D **44**, 1909 (1991).

[5] W.C. Chang and D. Dutta, Int. J. Mod. Phys. E **22**, 1330020 (2013).

[6] NA51 Collaboration, A. Baldit *et al.*, Phys. Lett. B **332**, 244 (1994).

[7] E866/NuSea Collaboration, R.S. Towell *et al.*, Phys. Rev. D **64**, 052002 (2001).

[8] W.C. Chang and J.C. Peng, Prog. Part. Nucl. Phys. **79**, 95 (2014).

[9] A. Bacchetta, F. Delcarro, C. Pisano, M. Radici and A. Signori, JHEP **1706**, 081 (2017).

[10] D. Boer, Phys. Rev. D **60**, 014012 (1999).

[11] COMPASS Collaboration, M. Aghasyan *et al.*, Phys. Rev. Lett. **119**, 112002 (2017).

[12] C.S. Lam and W.K. Tung, Phys. Rev. D **18**, 2447 (1978).

[13] C.S. Lam and W.K. Tung, Phys. Rev. D **21**, 2712 (1980).

[14] A. Brandenburg, O. Nachtmann and E. Mirkes, Z. Phys. C **60**, 697 (1993).

[15] Fermilab E866 Collaboration, L.Y. Zhu *et al.*, Phys. Rev. Lett. **99**, 082301 (2007); Phys. Rev. Lett. **102**, 182001 (2009).

[16] CDF Collaboration, T. Aaltonen *et al.*, Phys. Rev. Lett. **106**, 241801 (2011).

[17] CMS Collaboration, V. Khachatryan *et al.*, Phys. Lett. B **750**, 154 (2015).

[18] ATLAS Collaboration, G. Aad *et al.*, JHEP **08**, 159 (2016).

[19] R. Gauld, A. Gehrmann-De Ridder, T. Gehrmann, E. W. N. Glover and A. Huss, JHEP **1711**, 003 (2017).

[20] M. Lambertsen and W. Vogelsang, Phys. Rev. D **93**, 114013 (2016).

[21] J.C. Peng, W.C. Chang, R.E. McClellan, and O.V. Teryaev, Phys. Lett. B **758**, 384 (2016).

[22] W.C. Chang, R.E. McClellan, J.C. Peng, and O.V. Teryaev, Phys. Rev. D **96**, 054020 (2017).

[23] J. C. Peng, D. Boer, W. C. Chang, R. E. McClellan and O. Teryaev, arXiv:1808.04398 [hep-ph].

[24] COMPASS-II Proposal, CERN-SPSC-2010, `http://cds.cern.ch/record/1265628`.

[25] Paul E Reimer and the Fermilab SeaQuest Collaboration, J. Phys.: Conf. Ser. **295**, 012011 (2011).

[26] G. Altarelli, R. K. Ellis and G. Martinelli, Nucl. Phys. B **157**, 461 (1979); J. Kubar-Andre and Frank E. Paige, Phys. Rev. D **19**, 221 (1979); K. Harada, T. Kaneko and N. Sakai, Nucl. Phys. B **155**, 169 (1979); Erratum: Nucl. Phys. B **165**, 545 (1980).

[27] R. K. Ellis, G. Martinelli and R. Petronzio, Nucl. Phys. B **211**, 106 (1983); R. J. Gonsalves, J. Pawlowski and C. F. Wai, Phys. Rev. D **40**, 2245 (1989); P. B. Arnold and M. H. Reno, Nucl. Phys. B **319**, 37 (1989); Erratum: Nucl. Phys. B **330**, 284 (1990).

[28] S. Catani, L. Cieri, G. Ferrera, D. de Florian, M. Grazzini, Phys. Rev. Lett. **103**, 082001 (2009); S. Catani, M. Grazzini, Phys. Rev. Lett. **98**, 222002 (2007).

[29] K. Melnikov and F. Petriello, Phys. Rev. D **74**, 114017 (2006).

[30] D. Boer and W. Vogelsang, Phys. Rev. D **74**, 014004 (2006).

[31] E.L. Berger, J.W. Qiu, and R.A. Rodriguez-Pedraza, Phys. Lett. B **656**, 74 (2007); Phys. Rev. D **76**, 074006 (2007).

[32] DYNNLO v1.5, `http://theory.fi.infn.it/grazzini/dy.html`.

[33] A. Buckley, J. Ferrando, S. Lloyd, K. Nordstrm, B. Page, M. Rfenacht, M. Schnherr and G. Watt, Eur. Phys. J. C **75**, 132 (2015).

[34] Official LHAPDF6 PDF sets, `https://lhapdf.hepforge.org/pdfsets.html`.

[35] J.C. Collins and D.E. Soper, Phys. Rev. D **16**, 2219 (1977).

[36] B. Zhang, Z. Lu, B. Q. Ma and I. Schmidt, Phys. Rev. D **77**, 054011 (2008); Z. Lu and I. Schmidt, Phys. Rev. D **81** 034023 (2010).

[37] V. Barone, S. Melis and A. Prokudin, Phys. Rev. D **81**, 114026 (2010); V. Barone, S. Melis and A. Prokudin, Phys. Rev. D **82**, 114025 (2010).

[38] J. C. Peng, Proceedings for the "Transversity 2014" Workshop, EPJ Web Conf. **85**, 01009 (2015).

[39] A. Klein, X. Jiang *et al.* (Fermilab E1039/SeaQuest) (2013), Fermilab Proposal 1039, `http://www.fnal.gov/directorate/program_planning/June2013PACPublic/P1039_LOI_polarized_DY.pdf`.

[40] J.C. Collins, Phys. Rev. Lett. **42**, 291 (1979).

[41] R.L. Thews, Phys. Rev. Lett. **43**, 987 (1979).

[42] J. Lindfors, Phys. Scr. **20**, 19 (1979).

[43] X. Wang, W. Mao and Z. Lu, Eur. Phys. J. C **78**, 643 (2018).